DOI: 10.47743/achi-2022-1-0003 *ACTA CHEMICA IASI*, **30_1**, 45-88 (2022)

POLYANILINE SUPPORTED g-C_3N_4/CeO_2 FLUORESCENT CHEMOSENSOR FOR SELECTED HEAVY METAL AND NITRATE IONS DETERMINATION

Abdu Hussen Ali[a*], Isabel Diaz[b], Abebaw Adgo Tsegaye[c], Abi Taddesse Mengesha[a]

[a]*Department of Chemistry, Haramaya University; Dire Dawa, Ethiopia*
[b]*Instituto de Catalysis Petroleoquimica, CSIC, c/Marie Curie 2, Madrid 28049, Spain and Chemistry department, Addis Ababa University, Addis Ababa, Ethiopia*
[c]*Department of Chemistry, Bahir-Dar University; Bahidar, Ethiopia*

Abstract: The increasing of toxic heavy metal and nitrate ions contamination in water and food systems worldwide has become a core problem. Therefore, the development of real-time, highly sensitive and selective, simple technique for nitrate and toxic heavy metals ions (mercury, copper and arsenic) detection in water and food at ultralow concentrations are important for maintaining their safe deliveries to consumers. A highly efficient fluorescent chemosensor-based on polyaniline supported g-C_3N_4/CeO_2 nanocomposite for selective heavy metal and nitrate ions have been successfully developed in this research, by in situ polymerization method. The structural, morphological, and optical properties of the synthesized nanocomposites were characterized by using powder X-ray diffraction (XRD), Fourier- Transform Infrared spectroscopy (FT-IR), Scanning Electron Microscope (SEM), Photoluminescence (PL) and UV-Vis spectroscopy. In the absence of metal and nitrate ions, the nanocomposites exhibit high fluorescence intensity. However, the strong coordination of the basic sites to metal and nitrate ions, causes fluorescence quenching via photoinduced electron transfer and static quenching leading to the qualitative and quantitative detection of metal and nitrate ions. This fluorescent chemosensor exhibits high selectivity toward arsenic (III), copper (II), mercury (II) and nitrate ion. The sensor was more sensitive for copper (II) ion than arsenic (III), mercury (II) and nitrate ions because the Stern-Volmer quenching constants (K_{SV}) was found to be greater for copper

* Abdu, Ali, *e-mail:* abdelmelik9@gmail.com

(II) ion at ($3.25x10^4$ M^{-1}) compared to 8.12×10^3 M^{-1}, 2.93×10^4 M^{-1} and 3.19×10^2 M^{-1} for arsenic (III), mercury (II) and nitrate ions respectively. The practical use of this sensor for arsenic (III), copper (II), mercury (II) and nitrate ions determination in Coca-cola, tap water, milk and lettuce samples respectively, were also applied. The amounts of mercury and nitrate concentrations measured in milk and lettuce were 56.66 μM and 3.18 mM, exceeding the allowable limits stated by WHO (0.1 μM for mercury and 5.9 μM for nitrate, respectively).

Keywords: Chemosensor; Fluorescence quenching; Nanocomposite; Nitrate ion; Polyaniline; Toxic heavy metals

Introduction

Rapid economic development has generated contaminated industrial wastewater in developing countries, which has also led to water-related illnesses. The waste products generated from the textiles, chemicals, mining and metallurgical industries are mainly responsible for water contamination.[1] Such a waters usually contain non-biodegradable effluents, such as nitrate, heavy metal ions and toxic species (arsenic, zinc, copper, nickel, mercury, cadmium, lead, chromium, etc.), and organic materials carcinogenic for humans and harmful for the environment.[2,3] Nitrate (NO^{3-}) has been classified as an inorganic nitrogenous compound, able to cause diseases and becoming a threat to the human health. Nitrate ions can be found naturally in water, soil, and food, thus, making it easily consumed by humans.

Due to the nitrate excess, symptoms such as abdominal pain and diarrhea have also been observed in humans[4] and disruption of endocrine functioning of the thyroid gland are some of the prominent ill effects of nitrates.[5] On the other hand, heavy metal ions and chemicals, also harmful to the human body, contaminate the environment by emission into natural ecosystems, resulting in serious air, water, and soil pollution. Furthermore,

secondary pollution can result from the ingestion of plants and animals that inhabit the polluted environment, leading to the accumulation in the human body, thereby causing serious damage to human health and life.[6]

Among many heavy metal ions, copper ion is considered to be one of the critical heavy metal ions contained in drinking water, being a common contaminant produced by corrosion of household plumbing systems and erosion of natural deposits; it may induce gastrointestinal distress, even liver or kidney damage. Under overloading conditions, however, copper gets high toxicity to humans as disruption of homeostasis in cells and could cause oxidative stress and severe disorders such as Menkes syndrome, Wilson's disease, similar to Alzheimer's disease.[7] In addition, mercury is also one of the most toxic heavy metals in the environment, which tends to be accumulated in human body and result in severe damages in the nervous system, kidney failure and various cognitive and movement disorders.[8] Among various inorganic contaminants, arsenic was recently highlighted because of its high toxicity and complex geochemical behavior. The health effects of exposure to arsenic result in skin cancer and in various types of internal cancer, predominantly lung, bladder, and liver cancer.[9] Hence, it is required to develop tools or methods that can be used to determine the presence of these toxic elements and nitrate ions in various media such as water, food, biological, environmental, medical and industrial samples.

Conventional analytical techniques for heavy metal and nitrate detection exist, such as ion chromatography (IC), complexation electrospray mass spectrometry (cESI-MS), Raman spectroscopy,[10] inductively coupled plasma mass spectrometry (ICP-MS)[11], atomic absorption spectrometry (AAS)[12] and inductively coupled plasma optical emission spectrometry

(ICP-OES).[13] These methods offer good limits of detection and wide linear ranges, but require high-cost analytical instruments developed for use in the laboratories. The sample collection, transportation and pre-treatment is time-consuming and a potential source of errors. Recently, chemosensors have received a lot of attention due to their high sensitivity, selectivity, simplicity, low-cost instrumentation and field-work applicability for detection of heavy metal and nitrate ions. In particular, nanomaterials-based chemosensors have shown great promise due to their large surface area, high surface reactivity, and strong adsorption capacity.

A wide variety of nanomaterials such as metallic oxide nanoparticles and carbon-based materials have been widely used in the design of these sensors. The improved sensitivity of nanosensors is originated from their high reactivity, large surface to volume ratio, high degree of functionalization and size dependent properties.[14] Moreover, nanocomposite formation, covalent functionalization and organic ligand anchoring have also contributed largely to enhance the response sensitivity and selectivity in heavy metal and nitrate ions detection. The incorporation of semiconductor nanocomposite in a polymer matrix also was shown to result in improved mechanical, thermal, dielectric and optical properties, due to polymers providing of high carrier mobilities potential. In the fields of chemosensors, the organic sensing materials such as conducting polymers [polyaniline (PANI), polypyrrole (PPy), and polythiophene (PTP), etc.] can show response to target analytes at room temperature or low temperature, which has a convenient operating attractive prospect.[15]

Polyaniline (PANI) is unique among conducting polymers due to its chemical and environmental stability, good redox reversibility, tunable electrical conductivity and optical properties. These properties make it

favorable for applications in chemical sensors and the conversion of light to electricity. It has three different fundamental forms depending on the method employed for the preparation: leucomeraldine (fully reduced), emeraldine base (EB: half oxidized) and pernigraniline (fully oxidized). The only electrically conducting one is the emeraldine salt form (ES: half oxidized), which is the protonated form of PANI-EB.[16] There are only a few reports on the application of a simple concept, the fluorescence quenching of polyaniline and its derivatives in optical sensor studies; such as Cu/PANI for chloroform[17] and camphorsulfonic acid-doped polyaniline for NO_2 and O_2 gases as chemical sensing based on fluorescence quenching were studied.[18,19]

Metallic oxide nanoparticles-based sensors seem to be promising due to many unique properties that nanoscale materials offer. Among the different metallic nanoparticles, cerium oxide NPs has been highly focused on optical and photoelectronic properties for several years, depending on the size and morphology of the particle. Also, CeO_2 has a positive prospect on the luminescence properties due to its capacity of light absorption and the ability to emit through $O^{2-} \rightarrow Ce^{4+}$ transition. Nanoceria is optically active and can develop unique color patterns, depending upon specific interactions at their surface.[20] Therefore, one could combine the referred materials to enhance their luminescent properties. The optical properties of cerium oxide and gold-ceria nanoparticles and their uses for dissolved oxygen and lead metal ion detection, based on fluorescence quenching, were also reported.[21]

Graphitic carbon nitride is also the most stable polymorphic analog of carbon nitride, readily synthesized by calcining abundant nitrogen-rich precursors such as melamine, dicyandiamide, and urea. In addition, because of its high nitrogen content, g-C_3N_4 can provide more active reaction sites

than the other CN material and its lamellar structure favors the transport of electron. g-C_3N_4 also excellent biocompatibility, high photoluminescence (PL) intensity[22] and good photostability properties. All these unique characteristics make the g-C_3N_4 an ideal materials for photocatalysis, bioimaging and chemical sensing[23]. However, only a few studies have been reported concerning its application in the optical detection of environmental pollutants (for instance, it could be applied for fluorescence detection based on fluorescence quenching of Hg^{2+} [24], Cu^{2+} [25] and Fe^{3+}.[26]

The objective of this study is to design sensitive sensing material g-C_3N_4/CeO_2 by improving the sensing site of g-C_3N_4/CeO_2 for detection of selected metal and nitrate ions. In order to improve the sensing site of g-C_3N_4/CeO_2, polyaniline was used as a supporter. PANI based material has attracted a greater interest due to a light-harvesting and light-amplifying properties; possess high selectivity and binding efficiency due to incorporating of multiple recognition element for analyte.[27] Herein, this study aimed at g-C_3N_4/CeO_2 supported by polyaniline which prepared by in-situ polymerization method and assess the sensing performances towards the selected heavy metal and nitrate ions.

Experimental section

1. Materials

Aniline (Aldrich) was purified by distillation under reduced pressure prior to use. Cerium nitrate hexahydrate, sodium dihydrogen phosphate, disodium hydrogen phosphate, hydrochloric acid, urea, zinc dust, ethanol, ammonium persulfate, ammonia, copper sulfate, sodium arsenite, mercury nitrate, sodium sulfate, sodium bicarbonate, sodium chloride, sodium hydroxide, sodium nitrate, magnesium sulfate, potassium sulfate, calcium

sulfate, nickel nitrate, cobalt nitrate, ferrous sulfate, chrominium sulfate, cadmium nitrate and trichloro-acetic acid (Breckland) were used without purification.

2. Synthesis of nanocomposites

2.1. Synthesis of g-C_3N_4

Graphitic carbon nitride (g-C_3N_4) was synthesized by pyrolysis of urea in a muffle furnace. 25 g (0.416 mol) urea was put into an alumina crucible with a cover, heated up to 350 ^oC and kept at this temperature for 1 h. Further heating was performed up to 500 ^oC and kept here for 1 h. The heating rates were 10 ^oC min^{-1}. Finally, 1 g of a yellow powder (g-C_3N_4) was collected.

2.2. Synthesis of g-C_3N_4/CeO_2 nanocomposites

The g-C_3N_4/CeO_2 nanocomposite was synthesized based on literature[28] with minor modification. The g-C_3N_4 (0.1 g) and a certain quantity of $Ce(NO_3)_3 \cdot 6H_2O$ (0.0126 g) was added to 19 mL H_2O, and the suspension was stirred magnetically for 30 min and then sonicated for another 30 min. Subsequently, 0.5 mL of NH_4OH was injected into the mixture under magnetic stirring. The resulting product was separated by centrifuging and washed three times with distilled water and ethanol, then the product was dried at 60 ^oC for 2 h. Finally, the g-C_3N_4/CeO_2 product was collected and calcined in the muffle furnace at 300 ^oC for 1 h. The single cerium oxide ultrafine nanoparticles were prepared by a precipitation method.[29]

2.3. Synthesis of PANI/g-C_3N_4/CeO_2

A typical in situ polymerization method was adopted for the polymerization of aniline in the presence of g-C_3N_4/CeO_2 nanocomposite.

0.9313 g of g-C_3N_4/CeO_2 powder was added into 20 mL aqueous solution of 0.01 mol aniline monomer and 0.01 mol hydrochloric acid. 0.01 mol ammonium peroxy-sulfate was dissolved in 15 mL distilled water and added dropwise to the mixture of g-C_3N_4/CeO_2 and aniline, with stirring on an ice bath. Polymerization proceeded for 5.5 h. The composite of PANI-modified g-C_3N_4/CeO_2 was obtained as a precipitate. The precipitate was isolated by filtration, washed with distilled water and ethanol three times, then dried at 50 ^oC for 5 h. Pure PANI was also synthesized, by using an identical method, without using g-C_3N_4/CeO_2.

3. Characterization of the synthesized nanocomposites

To determine the characteristic maximum absorption of the as-synthesized samples and their band gaps, UV-Visible absorption spectrophotometer (SANYO SP65) was used in the range of 200-900 nm wavelength. The photoluminescence emission properties were determined using a RF-5301PC spectrofluorometer equipped with a xenon discharge lamp. The surface morphology was studied by scanning electron microscopy (SEM) using a Hitachi TM1000 instrument.The crystalline phases and the crystallite sizes were determined using powder X-ray diffraction (XRD) with X'Pert Pro PANalytical with CuKα radiation (λ = 1.5405 Å). The data were registered with 2θ steps of 0.02^o and accumulation times of 20 s. FT-IR (Spectrum 65, PerkinElmer) in the range 4000 - 400 cm^{-1} using KBr pellets was used to assign functional groups of as-synthesized PANI/g-C_3N_4/CeO_2.

4. Preparation of buffers

The 0.1 M phosphate buffer (PBS) was prepared by weighing approximately 0.8 g of $NaH_2PO_4.2H_2O$ and 6.5180 g of Na_2HPO_4 and

dissolving them in water into a 500 mL volumetric flask. It was adjusted using 0.1 M HCl or 0.1 M NaOH to the desired pH. The buffer solution was stored in a fridge at 4 ^oC.[30]

5. Fluorescence detection of selected heavy metal and nitrate ions

For fluorescence detection of selected heavy metal ions, in a typical run, 2.5 mL of PBS (0.1 M, pH 7.4) was added into 2 mg of the PANI/g-C_3N_4/CeO_2 nanocomposite, followed by the addition of different molar concentration of arsenic (III), copper (II) and mercury (II) and sonicated. For nitrate detection, 2 mg of the PANI/g-C_3N_4-CeO_2 nanocomposite was dispersed in 2.5 mL deionized water, followed by the addition of nitrate solution of different molar concentration, then sonicated. After 5 min reaction at room temperature, 50 µL of each solution prepared as described was taken into a cuvette. The excitation and emission spectra were recorded. In order to quantify the selected heavy metal and nitrate induced quenching process, the Stern-Volmer quenching constant K_{SV} was calculated by Stern-Volmer equation:

$$I_O/I = 1+K_{SV}[Q] \quad (1)$$

where I_O and I are the fluorescence intensities of the sensor in the absence and in the presence of metals and nitrate, respectively, K_{SV} is the Stern-Volmer constant and (Q) is the molar concentration of metal and nitrate.

6. Optimization of operating parameters

6.1. The effect of pH

The effect of pH (2-12) of phosphate buffer (PBS) on the PANI/g-C_3N_4/CeO_2 fluorescent chemosensor in the presence of selected heavy metal

solutions was tested, since it is well-known that the pH of a solution can affect the detection sensitivity and selectivity.

6.2. The effect of concentration

In order to investigate the effect of heavy metal and nitrate concentrations on the detection sensitivity, 2.5 mL of phosphate buffer (PBS) (0.1 M, pH = 6) was added to 2 mg the PANI/g-C_3N_4/CeO_2 nanocomposite, then 50, 200, 400, 600, 800 and 1000 μM of each metals solutions were added and the mixture was sonicated. For nitrate detection, 2 mg of the PANI/g-C_3N_4/CeO_2 nanocomposite was stirred in 2.5 mL deionized water, followed by the addition of 1, 2, 4, 6, 8 and 10 mM of nitrate and sonicated. After 5 min of reaction at room temperature, 50 μL of the solution was taken into a cuvette and the excitation and emission spectra were recorded using fluorescence spectroscopy.

7. Reproducibility and stability tests

The reproducibility of the PANI/g-C_3N_4/CeO_2 as the fluorescent sensor was investigated at three repetitions on three batches of the PANI/ g-C_3N_4/CeO_2. A calibration graph was plotted for the mean values of F_o/F, (F_o and F represent the fluorescence intensity of the sensor without and with metal and nitrate, respectively) versus metal and nitrate concentrations values. A linear range was then determined. The detection limit was calculated using the following formula:

$$\text{LOD} = \frac{3\ x\ SD}{K_{SV}} \qquad (2)$$

where LOD are the limit of detection, SD are standard deviation from linearity and K_{SV} is Stern-Volmer constant calculated from the graph.[31]

8. Selectivity of the sensor

The zinc (II), nickel (II), cobalt (II), magnesium (II), calcium (II), potassium (I), cadmium (II), chrominium (II) and iron (II) ions were used to investigate for selected heavy metal selectivity study, while SO_4^{2-}, Cl^-, OH^- and HCO_3^- ions were used to investigate selectivity for nitrate of PANI/g-C_3N_4/CeO_2 chemosensor. The concentration of each metal ion was 1000 μM and the concentration of each anion was 10 mM. The same detection conditions and approach were used in section 6.2.

9. Recovery test and real samples analysis

Coca-cola drink and tap water samples were collected from the supermarket and Gendemude, Haramaya Woreda. The tap water and coca-cola samples were spiked with different concentrations of Copper (II) and arsenic (III) solutions respectively. Typically 200 μL of each sample solutions was taken and added to PANI/g-C_3N_4/CeO_2 nanocomposite in 2.5 mL PBS (pH = 6). Finally, fluorescence emission spectra were recorded after 5 min of reaction at room temperature.

Furthermore, milk sample were collected from Haramaya University. The milk was treated as follows: 1% (w/v) Trichloro acetic acid was added and ultrasonicated for 20 min, to remove the protein; the sample was then centrifuged at 3,000 rpm for 10 min and filtered. The resultant milk samples were spiked with different concentration of mercury (II) solutions.[24] Then 200 μL of this sample solution was taken and added to PANI/g-C_3N_4/CeO_2 nanocomposite in 2.5 mL PBS (pH = 6). Finally, fluorescence emission spectra were recorded after 5 min of reaction at room temperature.

About 5 g of lettuce leaf sample was collected from the local market, Haramaya, Ethiopia for nitrate extraction. The lettuce leaf was torn into very small pieces and ground using pistil and mortar. The powder was added into a flask that contains 15 - 20 mL ethanol and sonicated for 15 minutes. The mixture was filtered through a Buchner funnel to separate the solid material, then the liquid was diluted with 5 mL of deionized water. The resultant samples were spiked with different concentrations of nitrate solutions. Then 200 µL of this sample solution was taken and added to PANI/g-C_3N_4/CeO_2 nanocomposite in 2.5 mL deionized water. Finally, fluorescence emission spectra were recorded after 5 min of reaction at room temperature.

The mean percentage recoveries for the arsenic (III), copper (II), mercury (II) and nitrate were calculated using the following equation:

$$\text{Percentage recovery} = \frac{CE}{CM} \times 100 \quad (3)$$

Where CE is the experimental concentrations determined from the calibration curve and CM is the spiked concentrations.

Results and discussion

1. Characterization of the chemosensor

The crystal structure of the as-synthesized composites was studied by powder X-ray diffraction (XRD), as shown in **Figure 1**. It is observed that two diffraction peaks at 2θ value of 27.5º and 13.1º corresponding to the (002) and (100) diffraction planes respectively for g-C_3N_4, which is in good agreement with previous reports (JCPDS 87-1526).[32] The stronger peak at 27.5º corresponds to the interlayer stacking of the aromatic systems and the weaker one at 13.1º which may be related to an in-plane tris-triazine

structural packing. The apparent peaks for CeO_2 are observed at 2θ values of 28.5º, 33.1º, 47.5º, 56.3º, 59.7º, 69.4º, 76.7º, 79.09º and 88.44º corresponding to the (111), (200), (220), (311), (222), (400), (313), (402) and (422) crystal planes of cubic crystalline phases respectively [96-434-3162].

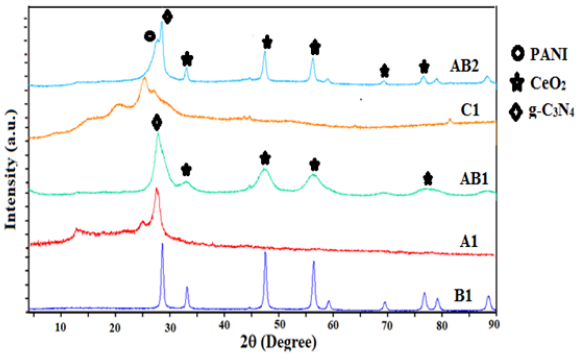

Figure 1. XRD patterns of the as-synthesized nanocomposites (where A1: g-C_3N_4, B1: CeO_2, C1: PANI, AB1: g-C_3N_4/CeO_2 and AB2: PANI/g-C_3N_4/CeO_2).

For g-C_3N_4/CeO_2 composites, the XRD patterns reveal a coexistence of both g-C_3N_4 and CeO_2. The reflections of CeO_2 nanoparticles from 28.5º assigned to the (111) plane are partly overlapped with the strong maximum of g-C_3N_4 at 27.5º. Moreover, the presence of CeO_2 nanoparticles on to g-C_3N_4 sheets have resulted in the disordered stacking of the nanocomposite. Therefore, the diffraction peak of g-C_3N_4/CeO_2 slightly shifted compared to the pure nanoparticles, which could be due to the crystal lattice distortion of g-C_3N_4, owing to the relatively strong interaction with CeO_2. The diffraction maxima observed at 2θ values of 27.53º is assigned to the (002) plane of g-C_3N_4, while the 32.77º, 47.2º, 55.9º and 68.9º signals are assigned to the (200), (220), (311) and (400) planes attributed to cubic CeO_2 crystal.

For pure PANI, the XRD pattern revealed three weak maxima at 2θ values of 15.1°, 20.53° and 25.36º, corresponding to the (111), (100) and (011) planes, attributed to the crystallographic planes for the emeraldine salt form of PANI, which is in a good agreement with other works.[33] The signal at 15.1° is attributed to the parallel repetition units of PANI, the one at 20.53° is usually due to the periodicity of the parallel and perpendicular polymer chains of PANI, while the peak at 25.36º is assigned to a periodicity caused by the H-bonding between PANI chains. The low intensity of the observed peaks indicate that PANI has semi-crystalline nature, due to the presence of a benzenoid and quinonoid group.[34]

The XRD diffraction of PANI/g-C_3N_4/CeO_2 nanocomposite consist of the major characteristics diffraction peak of PANI, g-C_3N_4, and CeO_2, with the 2θ values slightly shifted. The diffraction signal observed at 2θ values of 27.67º could be ascribed to PANI; 28.43º is attributed to g-C_3N_4 and the ones from 32.98º, 47.36º, 56.2º, 69.26º, 76.5º, 78.86º and 88.19º are due to CeO_2. The increase of the crystallinity degree compared to g-C_3N_4/CeO_2 nanocomposite is due to the strong interfacial interaction between the PANI and g-C_3N_4/CeO_2 nanocomposites. Therefore, the orientation of the conducting polymer nanocomposites is of high interest, due to higher ordered polymer matrix.

The average crystalline sizes (D) of all the five as-synthesized nanocomposites were calculated using the Debye-Scherrer's equation. [35]

$$D = \frac{k\lambda}{\beta \cos\theta} \quad (4)$$

where D is the mean crystallite dimension in nm, K is the crystallite shape factor constant (0.9), θ the Bragg angle in radians, λ is the wavelength of X-ray (0.15406 nm), and β the full width at half maximum (FWHM) of the

peak in radians. **Table 1** depicts the calculated values of crystal size of the as-synthesized chemosensor, labeled as A1, B1, C1, AB1 and AB2 for g-C_3N_4, CeO_2, PANI, g-C_3N_4/CeO_2 and PANI/g-C_3N_4/CeO_2 respectively from XRD analysis. The result indicated that the average crystal size of all as-synthesized nanocomposite were in nano rage. The average crystalline size of PANI/g-C_3N_4/CeO_2 was less than the single nanoparticle, however greater than g-C_3N_4/CeO_2 nanocomposite. This was may be due to the effect of polyaniline (PANI).

Table 1. The full width at half maximum (in radian) and crystal sizes of as-synthesized chemosensor.

Samples	Codes	θ (radian)	β (radian)	Average crystal size (nm)
g-C_3N_4	A1	0.239	0.01674	8.27
CeO_2	B1	0.249	0.00817	16.95
g-C_3N_4/CeO_2	AB1	0.240	0.02803	4.94
PANI	C1	0.221	0.00279	49.7
PANI/g-C_3N_4/CeO_2	AB2	0.247	0.0140	9.9

Figure 2 shows the SEM image to analyzed the surface morphologies of the as-synthesized nanocomposites. The SEM micrograph of CeO_2 indicate irregular sized particles with no distinct morphology. The same is valid for both bare binary g-C_3N_4/CeO_2 nanocomposite (Figure 2B) and PANI supported binary nanocomposite (Figure 2C). However, the white cloud-like material that appeared on both supported and unsupported binary nanocomposite is due to CeO_2.

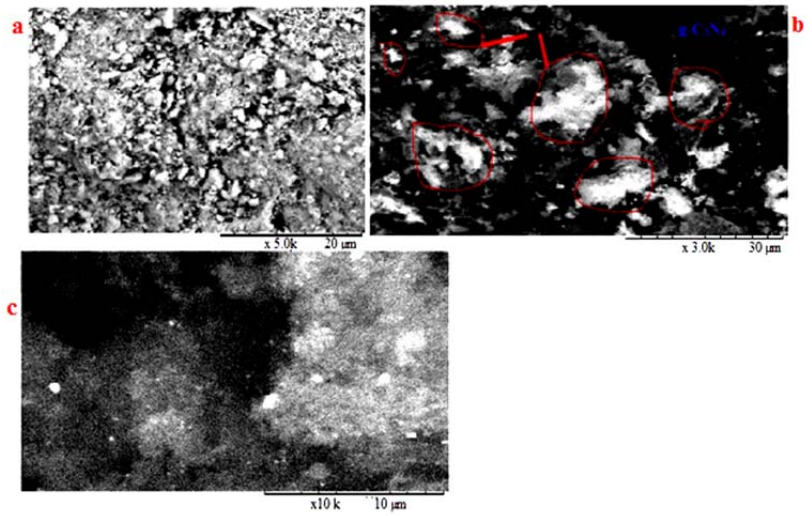

Figure 2. Typical SEM image of A) CeO_2, B) g-C_3N_4/CeO_2 and C) PANI/g-C_3N_4/CeO_2.

Figure 3 shows the FT-IR spectrum of the PANI/g-C_3N_4/CeO_2 nanomaterial. The result shows a broad absorption band located at 2970 - 3469 cm^{-1} corresponding to N-H stretching with hydrogen-bonded amino and imine site, and also free O-H stretching vibration of water. The peak appeared at 1638 cm^{-1} is due to C= C stretching mode of the quinoid rings, 1570 cm^{-1} due to C= C stretching mode of benzenoid rings due to the doped PANI. This indicated the presence of polyaniline in the synthesized nanomaterials. The peaks at 1242, 1322 and 1413 cm^{-1} are typical stretching vibration modes of C = N and sp^3 C – N bond of heterocycles. There is also a characteristics band at 806 cm^{-1}, attributed to the out-of plane breathing vibration characteristic of s-triazine units, these is in excellent agreement with samples of g-C_3N_4 produced via thermal polymerization reactions, including materials produced from oxygenated precursors such as urea. The characteristic band at 824 cm^{-1} is corresponding to out-of-plane bending vibration of C - H bond of *p*-disubstituted benzene rings of PANI[36] which confirms the head-to-tail

coupling of aniline units in the surface of g-C_3N_4/CeO_2. It can be observed that the bands corresponding to the characteristic of Ce-O stretching vibrations are at approximately 740 cm^{-1}, similar result has been reported in the other work.[37]

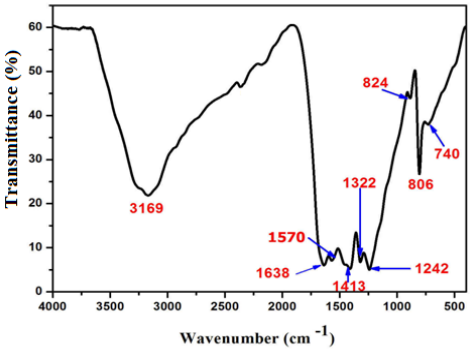

Figure 3. FT-IR spectra of PANI/g-C_3N_4/CeO_2 nanocomposite.

However, the CeO_2 absorption peak in PANI/g-C_3N_4/CeO_2 nanocomposites was less obvious, which may be attributed to the low content of CeO_2. Generally, the FT-IR results revealed that the characteristics peak of PANI, g-C_3N_4 and CeO_2 seem to be due to the formation of chemical bonding between the nanoparticles, instead of a simple physical attachment. This strong interfacial interaction can largely contribute to the charge transfer.

The optical absorption spectra of the synthesized nanocomposite was analyzed in the wavelength 200-900 nm range and the result is shown in Figure 4. The spectra show a well-defined absorption band at 307 nm, in the UV range, originating from the charge transfer transition from O^{2-}(2p) to Ce^{4+}(4f) orbital in CeO_2. g-C_3N_4 exhibits three absorption peaks at 280, 328 and 375 nm; the first and the last originate from $\pi \rightarrow \pi^*$ electronic transition in the aromatic 1, 3,5-triazine from g-C_3N_4 (C=N group) and from the

excitation n→π *, involving the lone pair of electrons on the nitrogen atoms (terminal N-C) respectively. These transitions involve planarity distortion of the s-heptazine ring of g-C_3N_4, favouring several n→ π* optical transitions.

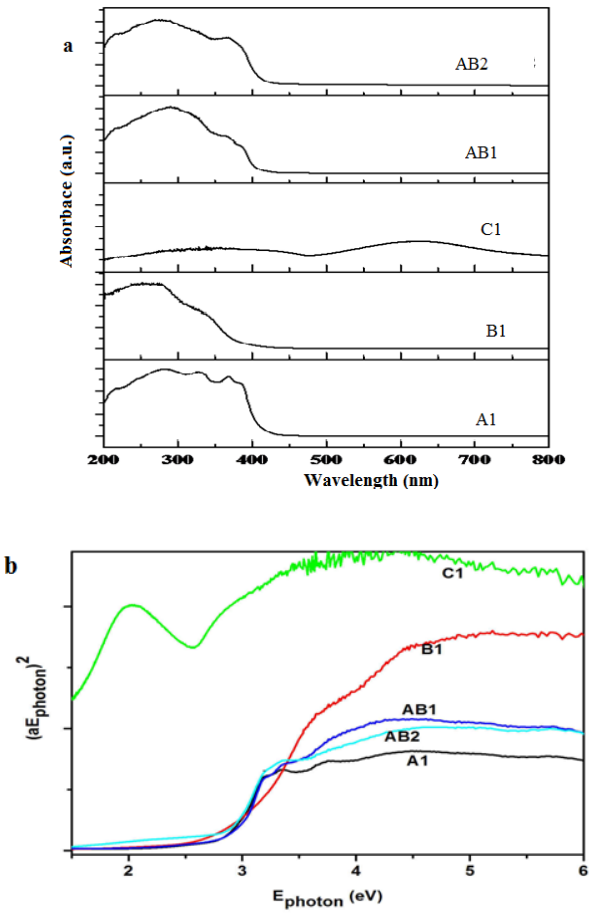

Figure 4. a) UV–vis DRS and b) Tauc plot for estimating the band gap energies of as-synthesized composites (where A1: g-C_3N_4, B1: CeO_2, C1: PANI, AB1: g-C_3N_4/CeO_2 and AB2: PANI/g-C_3N_4/CeO_2).

Pure PANI can absorb in both UV and visible spectrum region, due to transitions in the PANI molecules. The absorption reveals maximum at about 360 and 630 nm, which originate from the charge transfer excitation from the HOMO level to the LUMO energy level and the π–π* transition.[38]

The small absorption peak at 247 nm is attributed to the transition of an electron from the HOMO to LUMO which is related to π→π* electronic transition attributed to a local charge transfer between a quinoid ring and the adjacent imine-phenyl-amine units (intramolecular charge transfer exciton). The second peak at 360 nm which also indicates the presence of benzenoid group and lone pair of electrons of nitrogen. This, in turn, leads to π-π* interactions of the molecule and this shows that it is a conducting polymer.
It can be observed that after introducing wideband gap semiconductor CeO_2 into g-C_3N_4, the absorption edge of g-C_3N_4/CeO_2 composite is closer to 433 nm. Therefore, it displayed a slight blue shift in comparison with the g-C_3N_4.[39] It was deduced that the oxygen atoms in CeO_2 might be predictably doped in the g-C_3N_4 during the preparation process, leading to the disordered in-plane structural pattern of g-C_3N_4, delocalized p-electrons of oxygen atoms and the formation of intermediate energy levels by mixing of N 2p and O 2p orbital's, which would have an influence on the band positions of g-C_3N_4.

When the PANI is doped to g-C_3N_4/CeO_2, the absorption edge resulted in a slight red shift in comparison with the g-C_3N_4/CeO_2. This may occur because of interactions between PANI chains and g-C_3N_4/CeO_2 nanocomposite, which cause easy charge transfer from PANI to g-C_3N_4/CeO_2 *via* hydrogen bonding. The value of optical band gap decreased after doping. This may be due to a reduction in the disorder of the system and to an decrease of the density of defect states. Based on Kubelka-Munk equation,[40] the band gaps of the as-synthesized materials CeO_2, g-C_3N_4, PANI, g-C_3N_4/CeO_2 and PANI/g-C_3N_4/CeO_2 were found to be 3.06, 2.74, 1.7, 2.86, and 2.69 eV respectively.

2. Photoluminescence study

To understand the emission properties of the as-synthesized products, their photoluminescence (PL) properties were studied. **Figure 5** shows the emission of as-synthesized products at the same concentration under excitation of 360 nm using xenon laser. Pristine g-C_3N_4 (A1) exhibited a strong, broad peak centered at approximately 455 nm and with stronger intensity on account of the lone pair (LP) states in the valence band and π* antibonding states in the conduction band and the band gap energy closing to the energy of the excitation light.[41] The peak also becomes broader, which can be assigned to the band–band PL phenomenon with the energy of light approximately equal to the band gap energy of g-C_3N_4.[42] In fact, the band–band PL signal is attributed to excitonic photoluminescence, which mainly results from the $n \rightarrow \pi^*$ electronic transition that involves lone pairs of nitrogen atoms in g-C_3N_4.

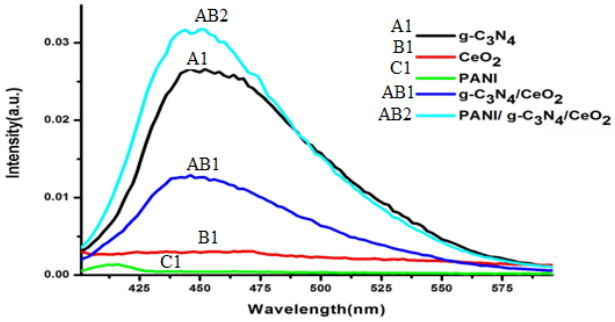

Figure 5. PL emission spectra of as-synthesized samples excited with wavelengths of 360 nm.

Cerium dioxide (CeO_2) has also a positive prospect on luminescence properties due to its capacity of light absorption and the ability to emit through $O^{2-} \rightarrow Ce^{4+}$ transition.[25] To explain the fluorescence emission properties of ceria exposed with 360 nm excitation causing the conduction

band electron to make a transition to defect state including oxygen vacancies, the electron undergoes multiple transitions in order to return to the ground state. The trivalent trap state of cerium ion is also correlated to fluorescence visible emission related to 5d - 4f energy level transition. It was found that PL emissions intensity is very weak. However, around 471 nm weak intense emission peaks, due to the different defect levels laid in the middle of Ce 4f and the O 2p were developed.

The photoluminescence intensity behavior of g-C_3N_4/CeO_2 nanocomposite has changed because the sign that the different interactions of g-C_3N_4 and CeO_2 in particles were different from spectra of pure particles, which results from mixing CeO_2 and g-C_3N_4 to form a stable mixture with perturbed energy levels. The enhanced emission peak was also noticed at 446 nm, a blue shift compared with pristine CeO_2 nanoparticle, due g-C_3N_4 mixing with CeO_2, lowering the activation energy of the O-vacancies inside the crystal structure of CeO_2. More trap trivalent cerium ion responsible for the enhancement of fluorescence emission were available. Polyaniline is also a fluorescence active molecule, showing emission peaks around 410 nm, due to π- π* transition of the benzene unit. The presence of distinct peaks in the PL spectra indicates the possibility of the existence of multiple electronic states participating in the photo-excitation process.[43] PANI exhibits weaker emission intensity than the others, this might be due to presence of additives that may reduce the possibility of aggregation in PANI.

As can be seen clearly from **Figure 5**, the fluorescence emission intensity of PANI/g-C_3N_4/CeO_2 nanostructures is higher than that of the other. Especially among these curves, the fluorescence curve of PANI displays the highest intensity at about 450 nm. This is due to the fact that a

coordination effect occurs between PANI and g-C_3N_4/CeO_2, and also possibly attributed to the change of the conjugated structure owing to the interaction of the nitrogen atom on PANI chains with the g-C_3N_4/CeO_2. Polyaniline-based fluorescent chemosensors can enhance and amplify the fluorescence responsive signal which was ascribed to unique π- π* conjugated electronic structure, allowing rapid energy/electron migration along the polymer backbone upon light excitations. Moreover, the exciton in PANI is highly mobile and diffuses in g-C_3N_4/CeO_2 by the mechanism that involves both through space dipolar coupling and strong mixing of the excited states. This gives rise to the higher density of states in the band gap resulting in increased PL intensity.

3. The Mechanism of the proposed fluorescent chemosensor

In order to investigate the performance of the PANI modified binary nanocomposites for the detection of selected heavy metal and nitrate ions, the interaction between sensor sites and the metal and nitrate ions were evaluated by the quenching effect study. The emission spectra were monitored at excitation wavelengths of 360 nm and the excitation spectra were monitored at an emission wavelength of 460 nm. The excitation and emission intensities of the PANI/g-C_3N_4/CeO_2 were quenched after addition of the nitrate ions. The decrease in the excitation and emission intensity can be attributed to the combined effect of decrease in absorbance at the excitation wavelength and to complex formation between the NO_3^- and the sensor. Nitrate is also considered an electron scavenger. This type of quencher probably involves the donation of electrons from the surface of PANI/g-C_3N_4/CeO_2 nanomaterial to the nitrate ion, deactivating the excited state responsible for fluorescence quenching.

The other possibility for fluorescence intensity quenching occurs due to the interactions between N and O sites in PANI/g-C_3N_4/CeO_2 with nitrate ions (non-covalent interactions like electrostatic or hydrogen bond for

chelation (NH/ N-O and Ce-O-N)). In addition, the nitrogen-containing groups (nitrogen site) from the PANI/g-C_3N_4/CeO_2 and nitrate ion might react to produce nitroso compounds, which results in fluorescence static quenching caused by chemical reactions.

On the other hand, the developed chemosensor was important for effective sensing of toxic heavy metal ions. Cu^{2+} can effectively quench the fluorescence intensities of PANI/g-C_3N_4/CeO_2 chemosensor, since Cu^{2+} is a paramagnetic ion with an unfilled d shell, where electron are transfered. In addition, the chelation of Cu^{2+} with the interaction site of the sensor brings them into close proximity to each other.[44] As a result, the redox potential of Cu^{2+}/Cu^{+} lies between the conduction band (CB) and valence band (VB) of PANI/g-C_3N_4/CeO_2, which resulted in photoinduced electron transfer (PET) from the CB to the complexed Cu^{2+} (**Figure 6**). Therefore, this leads to a rapid non- radiative decay of the excited PANI/g-C_3N_4/CeO_2, so the fluorescence emission intensities decreased.

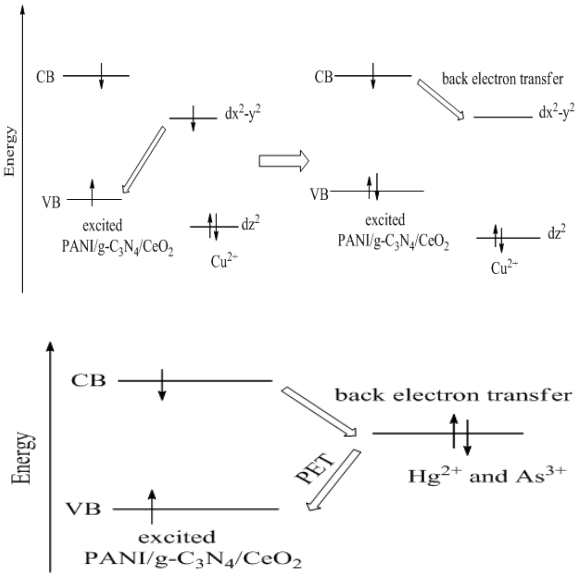

Figure 6. The proposed mechanism of PANI/g-C_3N_4/CeO_2 fluorescent chemosensor for metal ions and Electron-transfer fluorescence quenching.

The quenching of fluorescence intensity also observed upon addition of Hg^{2+} attributed to thereverse photo-induced electron transfer (PET) mechanism involving electron donation fromthe excited PANI/g-C_3N_4/CeO_2 part to the Hg^{2+} ion.[45] After Hg^{2+} had been added, the excited electron from the PANI/g-C_3N_4/CeO_2 may be transferred to the Hg^{2+}-bound which acted as an electron acceptor resulting in no fluorescence being observed (quenching). This mechanism was additionally supported by the fact that change in the emission spectra was observed, meaning that the quenching could not only be due to the interaction between the PANI/g-C_3N_4/CeO_2 in the excited state as the donor and the bound Hg^{2+} ion as the acceptor. The other quenching mechanism may be attributed to the electron energy transfer from the excited state of PANI/g-C_3N_4/CeO_2 to the d orbital of Hg^{2+}.[46] It was also suggested that PANI/g-C_3N_4/CeO_2 and Hg^{2+} form a covalent bond between Hg^{2+} and the interaction site in PANI/g-C_3N_4/CeO_2 (Hg–N) and (Hg–O) illustrating static quenching from the formation of a stable non-fluorescent complex between the PANI/g-C_3N_4/CeO_2 and Hg^{2+} ion. Therefore, the fluorescence of the synthesized sensor is significantly quenched. Generally, Hg^{2+} is a heavy metal ion, having an electronic configuration of $5d^{10}$ $6s^0$, and oxygen atoms or nitrogen atoms are good binding sites for it.

The quenching of excitation and emission intensity has also occurred after the addition of As^{3+} which may be due to the fact that arsenic is known to bind with the surface of the sensor molecules, rather than the edge site.[47] As a consequence, face-to-face stacking may occur, and this would quench fluorescence through radiationless decay mechanisms of the excited state of PANI/g-C_3N_4/CeO_2 fluorescent chemosensor. After the addition of As^{3+} solution, the PL intensity of PANI/g-C_3N_4/CeO_2 was quenched which was attributed to stronger affinity of interaction sites, specially interact with O

site (As–O) present on the surface of the nanocomposite. It can also induce the fluorescence quenching effect of PANI/g-C_3N_4/CeO_2 through intramolecular d-π interaction between the PANI supported g-C_3N_4/CeO_2 and As^{3+} ion. As well, the PANI/g-C_3N_4/CeO_2 has an electron donating group that can increase the electron cloud density of the system, and a π-electron cloud of the system enters the 3d orbital of arsenic, thereby making the combination of arsenic and the sensor molecule more stable. The proposed mechanism of the fluorescent chemosensor to metal and nitrate was described in figure 6.

Generally, the as-synthesized fluorescent chemosensor also has another site in PANI, in which the metal ion interaction occurs at the charged amine nitrogen sites rather than on the N site in the g-C_3N_4 , enhancing the detection system. CeO_2 also plays an important role that includes oxygen vacancies which can be adsorption center for heavy metal ions. This static association prevents the transfer of electrons on the conjugated chain, or induces ultrafast photoinduced electron transfer to the electron acceptor, resulting in the decrease of fluorescent intensity of the sensor material. Photoinduced electron transfer (PET) mechanisms are generally considered to play a significant role in the interaction of metal ions with the molecular orbital of the functional groups found in the as-synthesized chemosensor.

4. Optimization of experimental conditions

In order to evaluate the sensitivity of the proposed material, the experimental conditions were optimized including the pH of the buffer solution and concentration of metal and nitrate ions.

4.1. Influence of pH

The effect of pH on fluorescence response was carried out from pH 2- 12 at a concentration of 1 mM of each metal ion. The influence of pH on the quenching emission intensity of PANI/g-C_3N_4/CeO_2 by Hg^{2+}, As^{3+} and Cu^{2+} is described in **Figure 7**. The observed effect can be explained by acid-base equilibrium. The result indicate a shift to lower intensity on lower acidity, as well as the relative intensity ratio values decrease on going from pH 2 to pH 4. This is due to the fact that at lower pH, both interaction sites on PANI/g-C_3N_4/CeO_2 and the metal ions are fully protonated. Consequently, the complexation of Hg^{2+}, As^{3+} and Cu^{2+} is hindered because the necessary lone pair electrons are captured by the protons, thereby the weak interaction persists, characteristics of free ligand resulting in a low quenching efficiency.

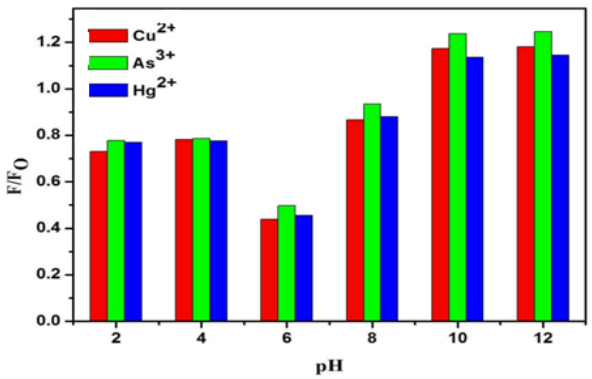

Figure 7. Fluorescence restoration of the PANI/g-C_3N_4/CeO_2 with Cu^{2+}, Hg^{2+} and As^{3+} ion in different pH solutions (0.1 M PBS).

As the pH increased from 4 to 6, the fluorescence intensity significantly decreased due to the high quenching efficiency and maximum quenching was observed at pH 6. This is due to the deprotonation of the interaction site, which increases the covalent bond strength between

PANI/g-C_3N_4/CeO_2 and the metal ions. As the pH further increases (pH ≥8), because of competitive metal hydroxide formation, it resulted in a distinct increase of the fluorescence intensity and thus a poor interaction with the sensor. Under basic solution, OH^- would react with Hg^{2+}, As^{3+} and Cu^{2+}, resulting in a low stability in this system. These results indicated that PANI/g-C_3N_4/CeO_2 is applicable to detect the selected metal ions in weakly acidic and neutral condition. Therefore, pH 6 is recommended as the optimal pH value for further detection.

4.2. The Concentration of metal ions

Since the PANI/g-C_3N_4/CeO_2 fluorescent chemosensor is fluorescent, the sensitivity of the emission behavior of the ultrasmall particles has been exploited for the determination of arsenic, copper and mercury ions in aqueous solution. The changes in the excitation and emission spectra of PANI/g-C_3N_4/CeO_2 was followed upon addition of different concentrations of these metal analytes as described in **Figure 8**. The fluorescence intensity of PANI/g-C_3N_4/CeO_2 quenches upon addition of these metal analytes. As described in the purposed mechanism (section 3.2), this is due to the properties of metal ions forming a reaction at the PANI/g-C_3N_4/CeO_2 surface, resulting in electron transfers. The prominent feature is that the intensity of excitation and emission is gradually quenched with an increase in the concentration of these metal analytes in aqueous solution. However, the fluorescence quenching test for copper indicates, a lower concentration of Cu^{2+} cannot quench the fluorescence intensity of the as-synthesized chemosensor thoroughly; when 50 μM copper ion solution was added there is no more quenching occuring but as the concentration was increased to 200 μM, the fluorescence quenching was observed clearly up to 1000 μM and the fluorescence intensity therefore decreases linearly.

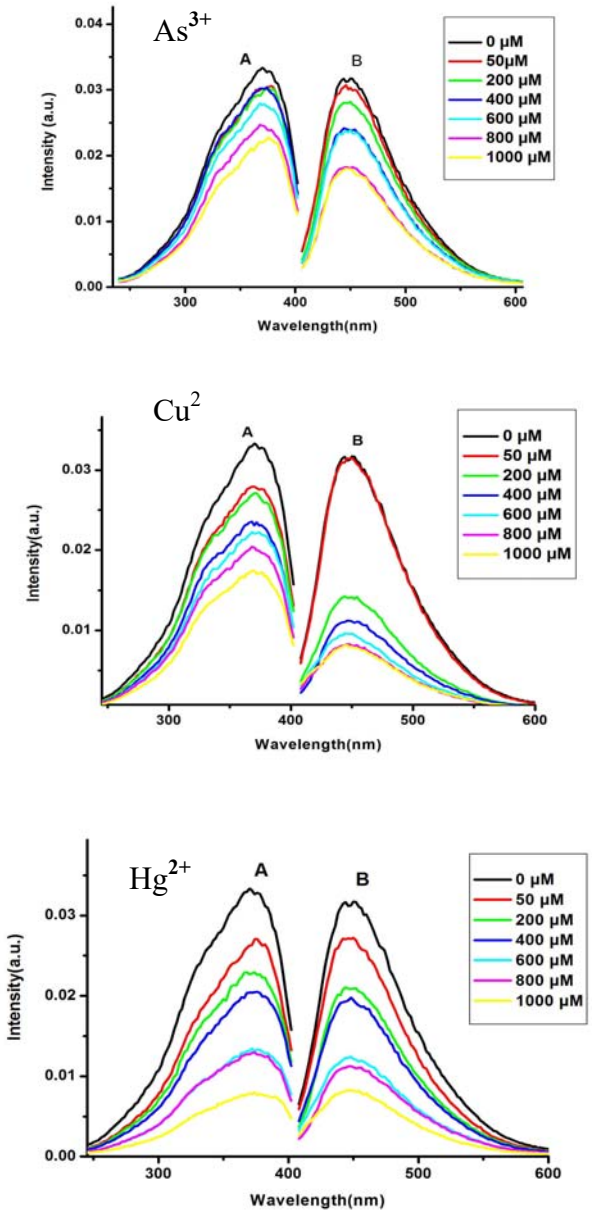

Figure 8. (A) excitation and (B) emission spectrum of PANI/g-C_3N_4/CeO_2 upon addition of As^{3+}, Cu^{2+}, and Hg^{2+} with various concentration.

Besides this, the excitation maximum for low concentration of arsenic and mercury ion becomes slightly red shifted. Upon careful

observation, it is conceived that the red shift for Hg^{2+} and As^{3+} are clear; this is because PANI/g-C_3N_4/CeO_2 contains an electron donating group conjugated to Hg^{2+} and As^{3+} able to undergo an intramolecular charge transfer on excitation by light. Usually, the donor and acceptor groups are conjugated in the ground state and undergo significant charge transfer in the excited state. It can be expected that the cations in close interaction with the donor or the acceptor moiety will change the properties of the sensor molecule because the complexed cation affects the efficiency of the intramolecular charge transfer. This results in changes of intensity and in spectral shifts of the excitation spectrum.

In addition to these, the dipole-ion coupling between the photoexcited PANI/g-C_3N_4/CeO_2 with Hg^{2+} and As^{3+} has also occurred. This is a radiationless process in which energy is transferred by coupling of the two oscillating dipole. The consequent change in dipole moment results in a spectral shift on the PANI/g-C_3N_4/CeO_2 material. The other possibility is when Hg^{2+} and As^{3+} are added to the chemosensor, the coordination-induced aggregation and electron transfer between these metal ions and PANI/g-C_3N_4/CeO_2 resulting in quenching of fluorescence and in a slight red shift in excitation/absorption spectrum.

4.3. The concentration of nitrate ion

In order to evaluate the PANI/g-C_3N_4/CeO_2 fluorescent chemosensor toward NO_3^- molecules, the quenching tests were conducted by monitoring the changes of the excitation and emission intensity in the presence of various concentrations of NO_3^- in the range of 1- 10 mM. As displayed in **Figure 9**, the intensities of the excitation and emission spectra of the PANI/g-C_3N_4/CeO_2 were found to decrease with the addition of NO_3^-, since

NO_3^- ion is not a fluorescence molecule. The reduced intensities suggested that the sensor sites excited at these excitation wavelengths interacted with NO_3^- molecule and the interactions led to the decrease in the emission intensity. While the red shifting of the excitation spectra at 2 mM (low concentration) may be ascribed to electron density changes caused by the complexation of NO_3^- and/or to conformational changes in the PANI/g-C_3N_4/CeO_2 backbone as a result of the chelation. The emission intensity of the PANI/g-C_3N_4/CeO_2 was found to decrease as the concentration of the NO_3^- increased up to 10 mM. Further increase in the concentration of NO_3^- did not cause a further decrease in the emission intensity. This is due to not all of the emission sites of the PANI/g-C_3N_4/CeO_2 could interact with the NO_3^- molecules because the nitrate group may be located several angstroms away from some interaction site, hence the nomenclature "non-coordinating". From this data 10 mM of nitrate ion was optimum concentration.

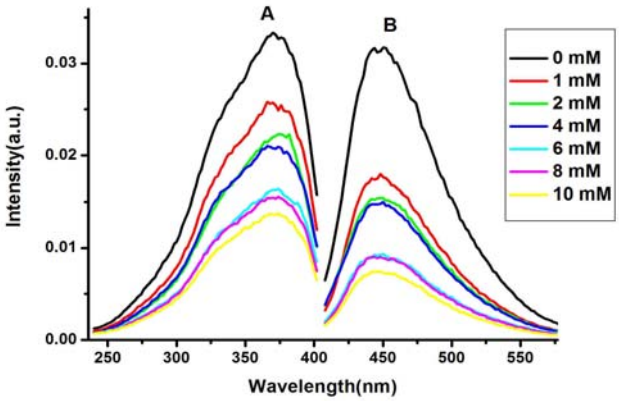

Figure 9. (A) excitation and (B) emission spectrum of PANI/g-C_3N_4/CeO_2 upon addition of NO_3^- ion with various concentration.

5. The sensitivity of the detection system

The detection of selected metal and nitrate ions were performed. The fluorescence intensity of PANI/g-C_3N_4/CeO_2 was found to be such that quenching and the Stern-Volmer fluorescence intensity ratio (F_O/F) show a linear diminish with the increasing As^{3+} and Hg^{2+} concentration from 50 μM to 1000 μM and Cu^{2+} from 200-1000 μM in a phosphate buffered solution (PBS, 0.1 M, pH = 6). On the other hand, the Stern-Volmer fluorescence emission intensity ratio (F_O/F) for nitrate ion is also linearly related with a concentration of 1-10 mM as shown in **Figure 10**. The fluorescence titration experiments showed that the metal and nitrate ions concentration is inversely proportional to fluorescence intensity, and gave a good linear change in Stern-Volmer fluorescence emission intensity ratio.

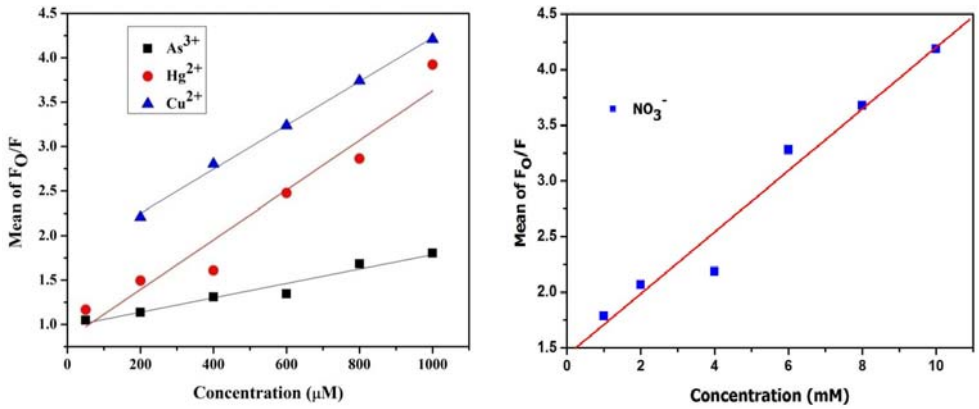

Figure 10. The reproducibility of the PANI/g-C_3N_4/CeO_2 responses excited at 360 nm for metal ion and NO_3^- concentration.

In order to clarify the favorable condition for the PANI/g-C_3N_4/CeO_2 to interact with the selected metal and nitrate ions

molecules, quenching efficiency at excitation wavelength was determined using a Stern-Volmer plot (eqn. 1).

In a fluorescent chemosensor, the emission intensity ratio can be defined as the response of the sensor. The sensing capability of the PANI/g-C_3N_4/CeO_2 was revealed from the slopes of the linear plots, corresponding to the quenching rate constants (K_{SV}). From the calibration curve, the linear dependence of the emission intensity on the concentration of As(III), Cu(II), Hg(II) and nitrate ions were deduced. Linear relationship with regression coefficients (R^2) of 0.948, 0.997, 0.931 and 0.98 were obtained for As(III), Cu(II), Hg(II) and nitrate ions, respectively. The sensitivity of the determination is directly related to the K_{SV} value (higher sensitivity means higher K_{SV} values). The calculated K_{SV} value for the PANI/g-C_3N_4/CeO_2 fluorescent chemosensor for As(III), Cu(II), Hg(II) and nitrate ions were found to be $8.12x10^3$ M^{-1}, $3.25x10^4$ M^{-1}, $2.93x10^4$ M^{-1} and $3.19x10^2$ M^{-1}, respectively; the proposed PANI/g-C_3N_4/CeO_2 fluorescent chemosensor was most sensitive to copper (II) ion.

In order to determine the LOD of the PANI/g-C_3N_4/CeO_2 fluorescent chemosensor, the reproducibility of the PANI/g-C_3N_4/CeO_2 in the linear range was checked by three repetitions. **Figure 10** also shows the reproducibility of the developed sensor at 360 nm excitation wavelength for each concentration of the selected metal and nitrate ions. The LOD of the PANI/g-C_3N_4/CeO_2 was determined from the standard deviation of the response at the intercept of the regression line and the value of the K_{SV}, (eqn. 2).

The detection limits for the proposed fluorescent chemosensors (As (III), Cu(II), Hg(II) and nitrate) were found to be $1.92x10^{-5}$, 4.11×10^{-6}, 2.08×10^{-5} and 3.3×10^{-4} M, respectively. The detection limit in this case was also good compared with those of the other fluorophore based fluorescent sensing methods as described in **table 2**.

Table 2. Comparing of the sensitivity of PANI/g-C_3N_4/CeO_2.

Mercury (II)			
Sensing material	Linear range	LOD (M)	Reference
Pyridine	0-50 μM	1.74 x 10^{-2}	[48]
Au- rhodium 6G	0-2.6 μM	6.0 x 10^{-5}	[49]
GCNNs	0-3.0 μM	3.0 x 10^{-4}	[24]
PANI/g-C_3N_4/CeO_2	0-1000 μM	2.08 x 10^{-5}	**This work**
Nitrate			
CN	0 -1800 μM	2.61 x 10^{-7}	[31]
GO	0-10 mM	-	[50]
EDTA-AgNPs	0 -2.5 μgmL^{-1}	1.8 x 10^{-4}	[51]
PANI/g-C_3N_4/CeO_2	0-10 mM	3.3 x 10^{-4}	**This work**
Arsenic (III)			
ZnO NPs	10-100 μM	2.8 x10^{-5}	[52]
Fe_3O_4 NPs	0-100 μM	3.0 x10^{-5}	[53]
PANI/g-C_3N_4/CeO_2	0-1000 μM	1.92 x 10^{-5}	**This work**
Copper (II)			
C-mpg-C_3N_4	10-100 μM	1.23 x10^{-8}	[23]
UGCNNs	0-10 μM	5.0 x10^{-10}	[25]
PANI/g-C_3N_4/CeO_2	200-1000 μM	4.11 x 10^{-6}	**This work**

6. Selectivity Test

6.1. Selectivity for metal ions

In addition to sensitivity, selectivity is another important parameter to evaluate the performance of the sensing system. The detection of heavy metal ions is usually accompanied by severe interferences of various ionic species. Therefore, the fluorescence features of the as-synthesized chemosensor were tested in the presence of competitive metal cations, other by Hg^{2+}, Cu^{2+} and As^{3+}, including Co^{2+}, Cd^{2+}, Fe^{2+}, Cr^{2+}, K^{+}, Ca^{2+}, Mg^{2+} and Ni^{2+}, under the same conditions. This selectivity test is important in order to investigate the selective interaction between PANI/g-C_3N_4/CeO_2 fluorescent chemosensor, necessary for practical applications. Metal salts solutions were added to the PANI/g-C_3N_4/CeO_2 in PBS and mixed to form

metal ion-PANI/g-C_3N_4/CeO_2 complexes. The chemosensor showed little significant responses to these metal ions, as described in **Figure 11**. This result suggests that the other metal ions only slightly quenched the fluorescence intensity of PANI/g-C_3N_4/CeO_2 compared with Hg^{2+}, Cu^{2+}, and As^{3+} ions, due to the weak affinity in the interaction with the PANI/g-C_3N_4/CeO_2 site.

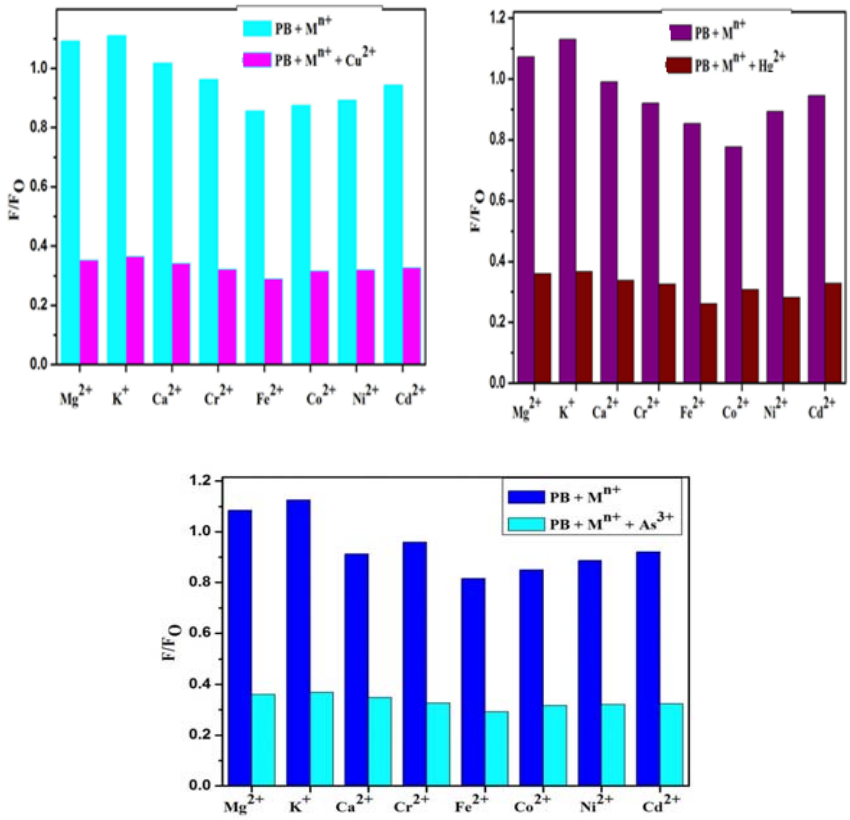

Figure 11. Fluorescence responses of PB (PANI/g-C_3N_4/CeO_2) upon treatment with 1 mM metal ion solutions and interference with Cu^{2+}, Hg^{2+} and As^{3+} (1 mM).

The slight quenching of emission occurs only when other metal than As, Cu and Hg were added. The higher concentration of the new-came metal ions induced a higher probability of collision between the excited species and metal ion during the lifetime of the excited state. The selectivity tests were completed by reaching the complete quenching, upon addition of

extra-amounts of Hg^{2+}, Cu^{2+} and As^{3+} in the the presence of the other mentioned metal ions. It showed that the other metal ions had a low influence on the interaction between copper, arsenic and mercury ions with the surface of the sensor within the range of measurements. The high chemosensor selectivity towards Hg^{2+}, Cu^{2+} and As^{3+} is attributed to the fact that they have higher thermodynamic affinity and faster chelating process with sensing site of PANI/g-C_3N_4/CeO_2 than the other metal ions.

6.2. Selectivity for nitrate ion

The selective sensing performance of PANI/g-C_3N_4/CeO_2 towards nitrate ions was evaluated on solutions containing also other anions, possibly interfering (SO_4^{2-}, HCO_3^-, Cl^- and OH^-). The interference extent for each anion was shown in **Figure 12**.

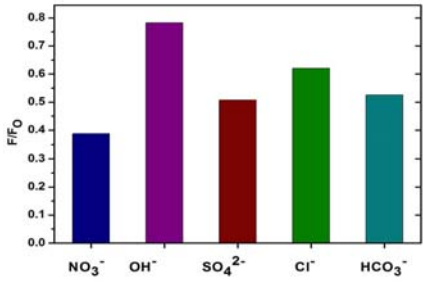

Figure 12. Selectivity of the PANI/g-C_3N_4/CeO_2 fluorescent chemosensor for NO_3^- ion. The concentration of all anions are 10 mM.

This result suggested that the detection of nitrate ions by PANI/g-C_3N_4/CeO_2 fluorescent chemosensor mostly influenced by OH^-, while the other ions displayed lower interference. The co-existence of polyatomic anions such as SO_4^{2-} and HCO_3^- with nitrate resulted in lower quenching activity of the PANI/g-C_3N_4/CeO_2 compared to HO^-. It is worthy noted that the PANI/g-C_3N_4/CeO_2 the chemosensor could be used to detect the nitrate ions even in the presence of OH^- ion.

7. Real samples fluorescence detection tests

The tap water, coca-cola drink, milk and lettuce samples were spiked with different concentrations of copper, arsenic, mercury and nitrate ions solutions to check the validity of the chemosensor functioning in real, complex liquids.

Calibration curves were obtained by using standard solutions of the fore-mentioned liquids spiked with metal and nitrate ions; three concentrations values were employed for each case. Excellent linear correlations between the contaminating metals concentrations (X) and F_O/F values (Y) measured from fluorescence spectra were obtained (Y = A + B X), respectively: As(III) $R^2 = 0.998$; Cu(II) $R^2 = 0.997$; Hg(II) $R^2 = 0.994$ and NO_3^- $R^2 = 0.913$, as displayed in **Figure 13**.

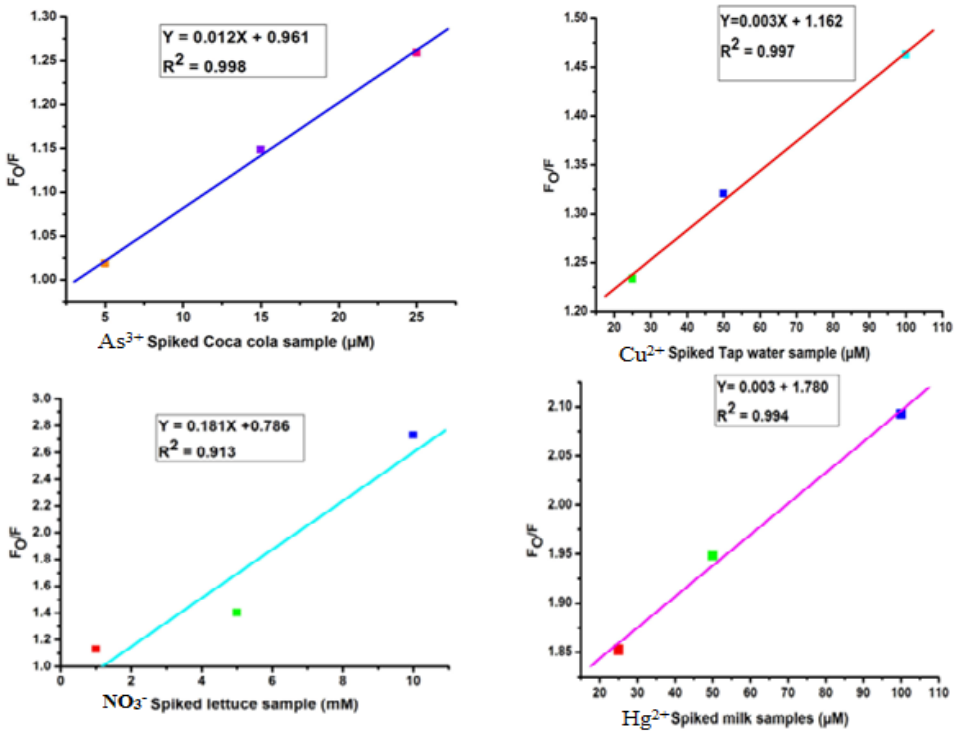

Figure 13. Calibration curves of F_O/F in real liquids at different toxic metals and nitrate ions concentration of (spiked samples).

8. Selected heavy metal and nitrate detection in real samples

Milk and lettuce real samples were measured using the described method and PANI/g-C_3N_4/CeO_2 fluorescent chemosensor for the detection of mercury and nitrate ion respectively (**Figure 14**).

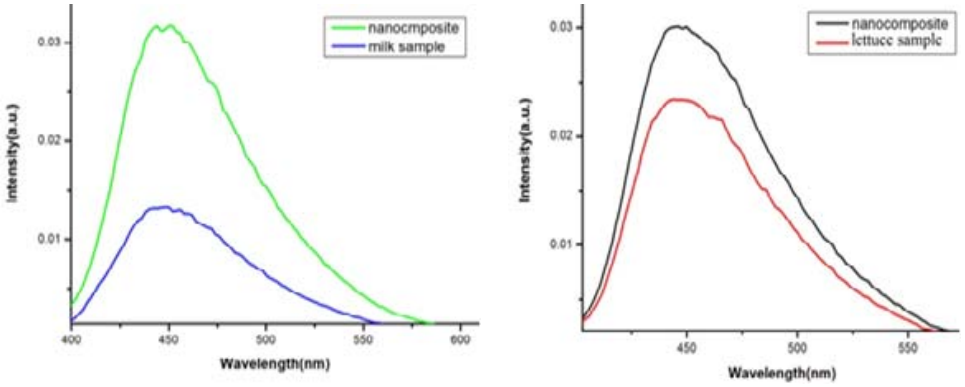

Figure 14. Fluorescence emission spectra of PANI/g-C_3N_4/CeO_2 with 200 µM of the milk and lettuce samples.

Unspiked coca-cola and tap water did not contain detectable amount of arsenic and copper ions. The results from fig. 14 is suggest that PANI/g-C_3N_4/CeO_2 fluorescent chemosensor has a promising prospect for the detection of these ions in real samples: the amounts of Hg (II) and nitrate found in milk and lettuce were found to be 56.66 µM and 3.18 mM, exceeding a lot (hundreds of time) the corresponding allowable limits of 0.1 µM and 5.9 µM stated by WHO. The contamination probably comes from the high levels of mercury and nitrate ions provided by the use of agro chemicals, reaching the soil and water, being successively transferred to plants and animals and finally deposited in their tissues. The nitrate contamination source is probably the use of chemical or animal manure a fertilizers, as well as the use of contaminated water for irrigation. The nitrate contaminated also comes from discharges of septic systems and municipal untreated wastewaters.

Conclusion

In this study, polyaniline supported g-C_3N_4/CeO_2 nanostructured chemosensor has been successfully developed for the determination of Cu^{2+}, Hg^{2+}, As^{3+}, and NO_3^- ions. The sensor was prepared by *in-situ* polymerization of polyaniline and g-C_3N_4/CeO_2. The materials were characterized by various techniques. The FT-IR, UV-Vis and XRD analysis confirmed that there is a strong interaction between PANI and the g-C_3N_4/CeO_2 nanocomposite.

The prepared fluorescent chemosensor was proved to be sensitive and selective towards Cu^{2+}, NO_3^-, Hg^{2+} and As^{3+} ions detection, by measuring the emission quenching and the excitation intensities of the chemical complexes formed between the sensor (PANI/g-C_3N_4/CeO_2) surface active sites and the fore-mentioned ions.

The developed sensor exhibited linear range, high selectivity and sensitivity towards low concentrations of the analyzed ions: As^{3+} (1.92×10^{-5}M); Cu^{2+} 4.11×10^{-6} M); Hg^{2+} 2.08×10^{-5} M) and NO_3^- 3.3×10^{-4} M. The detection was proved to work selectively also on complex fluids (tap water, soft drinks, milk, lettuce), delivering a relatively cheap, stable and environmental friendly fluorescent probe for rapid, highly selective and sensitive detection of several toxic ions.

Acknowledgments

I.D. expresses the deepest appreciation and thanks to Ministry of Education (MoE) of Ethiopia for providing me financial support, AAU for FT-IR analysis, Instituto de Catalysis Petroleoquimica of the Spanish Research Council (CSIC) for XRD, UV-Visible and SEM analysis of as-synthesized materials.

I.D. thanks the Department of Chemistry, HU for providing instruments and laboratory facilities as well as for facilitating required stuffs from the beginning to the completion of this study.

References

1. Rajkumar, D. and Jong, G.K. Oxidation of various reactive dyes with in situ electro-generated active chlorine for textile dyeing industry wastewater treatment. *J. Hazard. Mater. B.* **2006**, *136*, 203-212.
2. Kansal, S.K.; Singh, M. and Sud, D. Studies on photodegradation of two commercial dyes in aqueous phase using different photocatalysts. *J. Hazard. Mater.* **2007**, *141*, 581-590.
3. Shen, Y.F.; Tang, J.; Nie, Z.H.; Wang, Y.D.; Ren, Y. and Zuo, L. Preparation and application of magnetic Fe_3O_4 nanoparticles for wastewater purification. *Sep. Purif. Technol.* **2009**, *68 (3)*, 312- 319.
4. Namasivayam, C. and Sageetha, D. Removal and recovery of nitrate from water by ZnC_{l2} activated carbon from coconut coir pith, and agricultural solid waste. *Indian J. Chem. Technol.* **2005**, *12*, 513- 521.
5. Braverman, L.E.; He, X.; Pino, S.; Cross, M.; Magnani, B.; Lamm, S.H.; Kruse, M.B.; Engel, A.; Crump, K.S. and Gibbs, J.P. The effect of perchlorate, thiocyanate, and nitrate on thyroid function in workers exposed to perchlorate long term. *J. Clin. Endocrinol. Metab.* **2005**, *90 (2)*, 700-706.
6. Lim, S.H. and Yoon, S. Sensors and Devices for Heavy Metal Ion Detection. in *Smart Sens. Heal. Env. Moni.* **2015**, 213-232. Springer, Dordrecht.
7. Carter, K.P.; Young, A.M. and Palmer, A.E. Fluorescent sensors for measuring metal ions in living systems. *Chem. Rev.* **2014**, *114*, 4564-4601.
8. Mortazavi, S. M. J.; Mortazavi, G., and Paknahad, M. A review on the distribution of Hg in the environment and its human health impacts. *J. Hazard. Mater.* **2016**, *310*, 278- 279.
9. Yu, W.H., Harvey, C.M. and Harvey, C.F. Arsenic in groundwater in Bangladesh: A geostatistical and epidemiological framework for evaluating health effects and potential remedies. *Water Resour. Res.* **2003**, 39: 6
10. Niedzielski, P.; Kurzyca, I. and Siepak, J.A new tool for inorganic nitrogen speciation study: Simultaneous determination of ammonium ion, nitrite and nitrate by ion chromatography with post-column ammonium derivatization by Nessler reagent and diode-array

detection in rain water samples. *Anal. Chim. Acta* **2006**, *577(2)*, 220-224.

11. Zhu, Y.; Inagaki, K. and Chiba, K. Determination of Fe, Cu, Ni, and Zn in seawater by ID-ICP-MS after preconcentration using a syringe-driven chelating column. *J. Anal. At. Spectrom.* **2009**, *24*, 1179- 1183.

12. Pourreza, N. and Hoveizavi, R. Simultaneous preconcentration of Cu, Fe and Pb as methylthymol blue complexes on naphthalene adsorbent and flame atomic absorption determination. *Anal. Chim. Acta* **2005**, *549*, 124–128.

13. Chaiyo, S.; Chailapakul, O.; Sakai, T.; Teshima, N. and Siangproh, W. Highly sensitive determination of trace copper in food by adsorptive stripping voltammetry in the presence of 1, 10-phenanthroline. *Talanta* **2013**, *108*, 1- 6.

14. Li, M.; Gou, H.; Al-Ogaidi, I. and Wu, N. Nanostructured sensors for detection of heavy metals: a review. *ACS Sustain. Chem. Eng*. **2013**, *1*, 713-723.

15. Ma, X.F.; Mang, W.; Li, G.; Chen, H.Z. and Bai, R. Preparation of polyaniline-TiO_2 composite film with in situ polymerization approach and its gas-sensitivity at room temperature. *Mater. Chem. Phys.* **2006**, *98*, 241-247.

16. Masoumi, V.; Mohammadi, A.; Amini, M.; Khoshayand, M.R. and Dinarvand, R. Electrochemical synthesis and characterization of solid-phase microextraction fibers using conductive polymers: application in extraction of benzaldehyde from aqueous solution. *J. Solid State Electrochem.* **2014**, *18*, 1763-1771.

17. Sharma, S.; Nirkhe, C.; Pethkar, S. and Athawale, A.A. Chloroform vapour sensor based on copper/polyaniline nanocomposite. *Sens. Actuators B Chem*. **2002**, *85(1-2)*, 131-136.

18. Mohan, T.; Vijayadarshan, P.; Venkata, V.J.; Gupta, A.; Chowdary, T.V. and Venkataraman, A. Sensing of electron withdrawing group (-NO_2) in DNOC employing fluorescence of Camphorsulfonic acid doped Polyaniline (CSA-PANi) solution. *Int. J. Adv. Res. Innov. Ideas Educ.* **2017**, *3(4)*, 77- 83.

19. Draman, S.F.S.; Daik, R. and Ahmad, M. Synthesis and studies on fluorescence spectroscopy of CSA-doped polyaniline solution in DMF when exposed to oxygen gas. *Malaysian Polym. J.* **2009**, *4(1)*, 7-18.

20. Sharpe, E.; Frasco, T.; Andreescu, D. and Andreescu, S. Portable ceria nanoparticle-based assay for rapid detection of food antioxidants (NanoCerac). *Analyst* **2013**, *138*, 249-262.

21. Shehata, N.; Samir, E. and Kandas, I. Plasmonic-ceria nanoparticles as fluorescence intensity and lifetime quenching optical sensor. *Sensors.* **2018**, *18*, 2818 .

22. Huang, H.; Chen, R.; Ma, J.; Yan, L.; Zhao, Y.; Wang, Y.; Zhang, W.; Fan, J. and Chen, X. Graphitic carbon nitride solid nanofilms for selective and recyclable sensing of Cu^{2+} and Ag^{+} in water and serum. *Chem Commun*. **2014**, *50 (97)*, 15415-15418.

23. Lee, E.Z.; Jun, Y.S.; Hong, W.H.; Thomas, A. and Jin, M.M. Cubic mesoporous graphitic carbon (IV) nitride: An all-in-one chemosensor for selective optical sensing of metal ions. *Angew. Chem. Int. Ed.* **2010**, *49*, 9706- 9710.

24. Zhuang, Q.; Sun, L. and Yongnian, N. One-step synthesis of graphitic carbon nitride nanosheets with the help of melamine and its application for fluorescence detection of mercuric ions. *Talanta* **2017**, *164*, 458-462.

25. Tian, J.; Liu, Q.; Asiri, A.M.; Al-Youbi, A.O. and Sun, X. Ultrathin graphitic carbon nitride nanosheet: a highly efficient fluorosensor for rapid, ultrasensitive detection of Cu^{2+}. *Anal. Chem.* **2013**, *85*, 5595-5599.

26. Zhang, S.; Li, J.; Zeng, M.; Xu, J.; Wang, X. and Hu, W. Polymer nanodots of graphitic carbon nitride as effective fluorescent probes for the detection of Fe^{3+} and Cu^{2+} ions. *Nanoscale* **2014**, *6(8)*, 4157- 4162.

27. Kim, H.N.; Guo, Z.; Zhu, W.; Yoon, J. and Tian, H. Recent progress on polymer-based fluorescent and colorimetric chemosensors. *Chem. Soc. Rev.* **2011**, *40*, 79- 93.

28. She, X.; Xu, H.; Wang, H.; Xia, J.; Song, Y.; Yan, J.; Xu, Y.; Zhang, Q.; Du, D. and Li, H. Controllable synthesis of CeO_2/g-C_3N_4 composites and their applications in the environment. *Dalton Trans.* **2015**, *44(15)*, 7021-7031.

29. Gogoi, A. and Sarma, C.K. Synthesis of the novel β-cyclodextrin supported CeO_2 nanoparticles for the catalytic degradation of

methylene blue in aqueous suspension. *Mater. Chem. Phys.* **2017**, *194*, 327- 336.

30. Bisetty, K.; Sabela, M.I.; Khulu, S.; Xhakaza, M. and Ramsarup, L. Multivariate optimization of voltammetric parameters for the determination of total polyphenolic content in wine samples using an immobilized biosensor. *Int. J. Electrochem. Sci.* **2011**, *6*, 3631-3643.

31. Alim, N.S.; Lintang, H.O. and Yuliati, L. Fabricated metal-free carbon nitride characterizations for fluorescence chemical sensor of nitrate ions. *J. Eng. Sci. Technol.* **2015**, *76(13)*, 1-6.

32. Ye, L.; Liu, J.; Jiang, Z.; Peng, T. and Zan, L. Facets coupling of BiOBr-g-C_3N_4 composite photocatalyst for enhanced visible-light-driven photocatalytic activity. *Appl. Catal. B.* **2013**, *142*, 1-7.

33. Sonker, R.K. and Yadav, B.C. Development of Fe_2O_3–PANI nanocomposite thin film based sensor for NO_2 detection. *J. Taiwan Inst. Chem. Eng*. **2017**, *77*, 276-281.

34. Gu, L.; Wang, J.; Qi, R.; Wang, X.; Xu, P. and Han, X. A novel incorporating style of polyaniline/TiO_2 composites as effective visible photocatalysts. *J. Mol. Catal. A Chem.* **2012**, *357*, 19-25.

35. [35] Petkowicz, D.I.; Pergher, S.B.; Da Silva, C.D.S.; Da-Rocha, Z.N. and Dos Santos, J.H. Catalytic photodegradation of dyes by in situ zeolite-supported titania. *Chem. Eng. J.* **2010**, *158(3)*, 505-512.

36. Ayad, M.M.; Salahuddin, N.A.; Minisy, I.M. and Amer, W.A.Chitosan/ polyaniline nanofibers coating on the quartz crystal microbalance electrode for gas sensing. *Sens. Actuators B.* **2014**, *202*, 144-153.

37. Thakur, S. and Patil P. Rapid synthesis of cerium oxide nanoparticles with superior humidity-sensing performance. *Sens. Actuators B Chem.* **2014**, *194*, 260- 268.

38. Singh, S.; Rama, N. and Rao, M.S.R. Influence of d–d transition bands on electrical resistivity in Ni doped polycrystalline ZnO. *Appl. Phys. Lett.* **2006**, *88(22)*, 222111-222113.

39. Sun, J.; Zhang, J.; Zhang, M.; Antonietti, M.; Fu, X. and Wang, X. Bioinspired holloe semiconductor nanospheres as photosynthetic nanoparticles. *Nat. Commun Cat.* **2012**, *3*, 1139.

40. Liu, Z.; He, W. and Guo, Z. Metal coordination in photoluminescent sensing. *Chem. Soc. Rev.*. **2013**, *42 (4)*,1568-1600.

41. Zhang, Y.; Pan, Q.; Chai, G.; Liang, M.; Dong, G.; Zhang, Q. and Qiu, J. Synthesis and luminescence mechanism of multicolor-emitting g-C_3N_4 nanopowders by low temperature thermal condensation of melamine. *Sci. Rep.* **2013**, *3*, 1943.

42. Gu, L.; Wang, J.; Zou, Z. and Han, X. Graphitic-C_3N_4-hybridized TiO_2 nanosheets with reactive {0 0 1} facets to enhance the UV and visible-light photocatalytic activity. *J. Hazard. Mater.* **2014**, *268*, 216- 223.

43. Sharma, M.; Kaushik, D.; Singh, R.R. and Pandey, R.K. Study of electropolymerised polyaniline films using cyclic voltammetry, atomic force microscopy and optical spectroscopy. *J. Mater. Sci.:Mater. Electron.* **2006**, *17(7)*, 537-541.

44. Zong, C.; Ai, K.; Zhang, G.; Li, H. and Lu, L. Dual-emission fluorescent silica nanoparticle-based probe for ultrasensitive detection of Cu^{2+}. *Anal. Chem.* **2011**, *83 (8)*, 3126- 3132.

45. He, C.; Zhu, W.; Xu, Y.; Chen, T. and Qian, X. Trace mercury (II) detection and separation in serum and water samples using a reusable bifunctional fluorescent sensor. *Anal. Chim. Acta.* **2009**, *651 (2)*, 227-233.

46. Tan, H. L.; Liu, B. X. and Chen, Y. Lanthanide coordination polymer nanoparticles for sensing of mercury (II) by photoinduced electron transfer. *ACS Nano*. **2012**, *6*, 10505-10511.

47. Barone, P.W.; Baik, S.; Heller, D.A. and Strano, M.S. Near-infrared optical sensors based on single-walled carbon nanotubes. *Nat. Mater.* **2005**, *4(1)*, 86-92.

48. Pan, J.T.; Zhu, F.; Kong, L.; Yang, L.M.; Tao, X.T.; Tian, Y.P.; Lu, H.B. and Yang, J.X. A simple pyridine-based colorimetric chemosensor for highly sensitive and selective mercury (II) detection with the naked eye. *Chem. Pap.* **2015**, *69 (4)*, 527-535.

49. Chen, J.; Zheng, A.; Chen, A.; Gao, Y.; He, C.; Kai, X.; Wu, G. and Chen, Y.A functionalized gold nanoparticles and Rhodamine 6G based fluorescent sensor for high sensitive and selective detection of mercury (II) in environmental water samples. *Anal. Chim. Acta* **2007**, *599*, 134-142.

50. Tang, H.; Sundari, R.; Lintang, H.O. and Yuliati, L. Detection of nitrite and nitrate ions in water by graphene oxide as a potential fluorescence

sensor. *In IOP Conference Series: Mater. Sci. Eng.* **2016**, *107*, 012027.

51. Wang, C.C.; Luconi, M.O.; Masi, A.N. and Fernández, L.P. Derivatized silver nanoparticles as sensor for ultra-trace nitrate determination based on light scattering phenomenon. *Talanta*. **2009**, *77(3)*, 1238-1243.

52. Pal, S.K.; Akhtar, N. and Ghosh, S.K. Determination of arsenic in water using fluorescent ZnO quantum dots. *Anal. Methods* **2016**, *8(2)*, 445- 452.

53. Liu, B. and Liu, J. DNA adsorption by magnetic iron oxide nanoparticles and its application for arsenate detection. *Chem.Comm.* **2014**, *50(62)*, 8568 - 8570.